ARTICLE

Fluoro-silsesquioxane-urethane Hybrid for Thin Film Applications

Aravindaraj G Kannan, Namita Roy Choudhury,* and Naba Dutta

Ian Wark Research Institute, ARC Special Research Centre for Particle and Material Interfaces, University of South Australia, Mawson Lakes, South Australia 5095, Australia

ABSTRACT New fluoropolyurethane hybrids containing fluorinated polyhedral oligomeric silsesquioxane were synthesized for thin film applications using fluoro(13) disilanol isobutyl-POSS (FluoroPOSS) and a short chain fluorodiol and diisocyanate. The kinetics of the urethane reaction was monitored using Fourier transform infrared spectroscopy (FTIR) and the formation of urethane was confirmed using ^{29}Si Nuclear magnetic resonance spectroscopy (NMR). The effect of addition of FluoroPOSS either in the I step or II step of the two step polymerization reaction is evaluated using various spectroscopic, thermal, microscopic, and diffraction techniques. In general, the major shortcoming of the lack of flexibility of fluoropolyurethane from short chain diol and diisocyanate has been overcome by the use of tethered FluoroPOSS. X-ray photoelectron spectroscopy (XPS), atomic force microscpopy (AFM), and contact angle measurements on the hybrid thin films on silicon wafer demonstrate the migration of FluoroPOSS segment to the air-thin film interface when FluoroPOSS is used in I stage reaction, and it resides at the interface when used as a chain extender. However, in both cases, the formed thin film exhibits ultrahydrophobicity with water contact angle of approximately 107° and low contact angle hysteresis and solvent resistance, which are preferable for protective thin film applications.

KEYWORDS: FluoroPOSS • polyurethane hybrid • silsesquioxanes • thin films • ultrahydrophobicity

INTRODUCTION

Polymers that contain fluorocarbon chain in or along the backbone are attractive candidates for various high performance applications, especially as thin films, due to their versatile nature and their unique combination of several useful properties such as low surface energy, low coefficient of friction, excellent environmental stability, biocompatibility and resistance to chemical attack (1). A thin layer of hydrophobic fluorinated segment on the surface along with the control of surface texture can greatly enhance nonwetting behavior with respect to water. Such surfaces exhibit characteristic properties such as low adhesion, low friction and good biocompatibility, which are useful for many applications including antifouling and self-cleaning coatings, biomedical devices, microfluidic systems and tribological surfaces (2−5). Artificial water repellent characteristics have thus been introduced on a variety of surfaces by a number of ways such as incorporating a thin layer of fluorocarbon on the surface using self-assembled monolayers (6), blends (7), copolymers (2) and functional nanoparticles (8) through plasma processing, sputtering, spin coating, dip coating, self-assembling techniques and by creating roughness.

While fluorinated compounds are the most suitable category of materials to create hydrophobicity, polyhedral compounds could also be the obvious choice for such characteristics because of their molecular level roughness. Among various types of polyhedral compounds (9, 10), fluorinated polyhedral oligomeric silsesquioxane (POSS) has recently attracted significant interest to prepare oil/water repellent surfaces because of its remarkable surface and bulk properties (11). A typical fluorinated POSS has a POSS structure (silicon−oxygen cage structure surrounded by organic and/or reactive functionalities) with one or more peripheral organic groups replaced by fluorocarbon chains. It can have open cage or closed cage structure. This nanostructured material possesses highest density, highest molecular weight and lowest surface tension of all POSS compounds. Fluorinated POSS nanostructure acts not only as reinforcing agent in the polymer but also enhances surface properties. Apart from this, POSS bearing covalently bonded reactive functionalities can react with polymer chains or reactive monomers to form highly ordered unique hybrid materials suitable for various advanced applications, ranging from coatings to catalysis (12). The versatility of the POSS molecules results from their high thermal stability, oxidation resistance, discrete molecular weight, and tailoring of the number of reactive sites that allow controlled functionalization (11,13−15).

Tuteja et al. (16) recently synthesized fluorinated POSS materials containing fluoroalkyl groups and blended with PMMA to design superhydrophobic and superoleophobic surface. The authors have reported that to form superoleophobic surface, a third factor re-entrant surface curvature along with chemical composition and surface roughness are required. In other instance, fluorinated POSS capped polyethylene oxide was incorporated into epoxy resin, where the authors observed significant migration of the fluorinated POSS moiety at the surface of the thermoset (17). Due to their limited solubility, often fluorinated materials are blended with other materials to achieve hydrophobicity. Moody et al. (18) blended fluorinated and nonfluorinated POSS with

* Corresponding author. Phone: 61 8 8302 3719. Fax: 61 8 8302 3755. E-mail: Namita.Choudhury@unisa.edu.au.

Received for review September 16, 2008 and accepted November 30, 2008

DOI: 10.1021/am800056p

Published on Web 01/14/2009

different polymer matrices by melt mixing and demonstrated that the fluorinated POSS blends drastically increased the hydrophobicity and oleophobicity of those materials.

However, to date, to the best of our knowledge, no attempt has been made to utilize the beneficial properties of the fluoropolymer or fluoropolyurethane with the fluorinated POSS to make hybrid samples suitable for thin film applications. Polyurethanes (PU) are one of the most widely used polymers for thin film and coating applications and are well-known for their toughness, resistance to chemicals and solvents, glossy finish, and durability.

Because of the availability of a wide variety of isocyanates and hydroxyl end groups, a broad spectrum of materials can be produced with various mechanical and physiochemical characteristics. These coatings often show inherent weaknesses such as hydrophilic characteristics, low thermal stability, high coefficient of friction, and mechanically weak films, which we expect to overcome by incorporating fluorinated POSS components in the polyurethane matrix. The synthesis of fluorinated PU is often limited because of the availability of fluorinated hydroxy or isocyanate compounds. 2,2,3,3,4,4,5,5-Octafluoro-1,6-hexanediol (OFHD)-based PU has been reported using nonfluorinated diisocyanate. Also, the major shortcomings of such PU prepared from short-chain fluorodiol and diisocyanate are the lack of flexibility and hydrophobicity. To overcome this, we have synthesized an entire new series of fluoropolyurethane using fluorinated POSS components. We have combined the major attributes of urethane with fluorinated nanostructured material by utilizing open-caged fluoro(13) disilanol isobutyl-POSS (henceforth referred as FluoroPOSS) structure containing two functional hydroxyl groups, which can form urethane linkage with short chain isocyanates followed by chain extension with short chain fluorinated diol to develop fluoro-silsesquioxane-polyurethane hybrid. The rationale behind using short chain diols/diisocyanates is to eliminate the effect of long chain fluorinated compounds such as its extremely low reactivity and to use the synthesized hybrids as model compounds to investigate the effect of nanostructured FluoroPOSS on the hydrophobicity of thin film. The ultimate aim is to prepare a hydrophobic, solvent resistant, hybrid thin film with low surface energy. Also, the effect of fluoroPOSS either in the polymer backbone or as an endcapping agent is examined to elucidate its effect on hydrophobic properties of the final film.

EXPERIMENTAL SECTION

Materials. Hexamethylene diisocyanate (HDI), 2,2,3,3,4,4,5,5-Octafluoro-1,6-hexanediol (OFHD), anhydrous tetrahydrofuran (THF) solvent and dibutyl tin dilaurate (DBTDL) catalyst were purchased from Aldrich, Australia. Fluoro(13) disilanol isobutyl-POSS (molecular weight = 1195 AMU) was purchased from Hybrid Plastics, USA. All the chemicals were used as received without further purification.

Stage I: Synthesis of Isocyanate Terminated Prepolymer (Fluoropolyurethane). The isocyanate terminated fluoropolyurethane was synthesized by the reaction of HDI with fluoroPOSS at a stoichiometric molar ratio of 2.2:1 (HDI:fluoroPOSS). DBTDL was used as a catalyst. In a typical reaction, 2 mmol of fluoroPOSS dissolved in THF was taken in a dry, three-necked, round-bottom flask fitted with a condenser and a magnetic stirrer. The solution was stirred during the dropwise addition of 4.4 mmol of HDI in THF at ambient conditions for 10 min. The flask was then immersed in an oil bath maintained at 75 ± 1 °C to carry out the reaction. The progress of the reaction was monitored from the decrease in the isocyanate peak at 2269 cm^{-1} via transmission FTIR. The reaction was deemed partially complete when the isocyanate peak intensity was reduced to 50% of its original intensity. Because the sample quantity was different in each spectroscopic analysis, the Si—O—Si peak from fluoroPOSS core structure was used as an internal standard to normalize the isocyanate peak and calculate the consumption of isocyanate groups during urethane formation.

Stage II: Chain Extension of Prepolymer with OFHD. In the second stage, 2 mmol of OFHD dissolved in dry THF was added dropwise to the prepared fluoropolyurethane prepolymer (NCO:OH 1:1) solution. The reaction was carried out at 75 ± 1 °C under constant stirring. Again, the reaction was monitored via transmission FTIR and the completion of the reaction was monitored from the disappearance of the isocyanate peak. The resultant hybrid (henceforth referred as hybrid-1) was precipitated in water. The dried hybrid was purified by washing with THF several times to remove any unreacted monomer and dried in a vacuum oven at 40 °C for 4 h to remove the solvent. The dried bulk material was used for further spectroscopic, thermal, X-ray crystallographic, and elemental analyses. Similar two-step procedure was followed to synthesize fluoroPOSS endcapped hybrid (henceforth referred as hybrid-2) by forming prepolymer from short chain diol and diisocyanate and further chain extending the prepolymer with fluoroPOSS. A representative scheme of hybrid-2 synthesis is shown in Scheme 1.

Thin Film Coating. Hybrid thin films were applied on silicon wafer substrate using the following procedure: (a) silicon wafers were cleaned by immersing in 30% KOH solution for 20 s, (b) wafers were then rinsed with distilled water and dried at 80 °C for 3 h. The purpose of this step was to produce a fresh oxide layer for chemical bonding to the functional groups of the hybrid urethane. The prepared silicon wafer substrates were then dip-coated by 5% m/v partially reacted (at 75% isocyanate consumption) hybrid solution in dry THF for 2 min and then dried with pure nitrogen. Similarly, FluoroPOSS films were formed on treated silicon wafers using 5% m/v FluoroPOSS solution in dry THF for 2 min by dip coating. The coated samples were placed in an oven at 80 °C for 1 week for curing. This curing step serves the purposes of carrying out the remaining reaction on the substrate and annealing the sample to minimize the free energy. At room temperature, the polymer coating might otherwise take a long time to achieve equilibrium morphology depending on their composition. Annealing of the samples at higher temperature increases the mobility of the molecules thereby permitting the reordering of the surface structure to achieve equilibrium morphology (19). The evaporation of remaining solvent and the residual reaction resulted in optically transparent films. The coated samples were then subjected to solvent rinsing using THF to remove any physisorbed layers. The post cured coated samples were dried and then utilized for further surface characterizations.

Spectroscopic Characterization. The spectroscopic characterization of the monomers and the progress of the reaction were monitored using Transmission mode FTIR. Sodium chloride plates were used as window material. The synthesized hybrids were characterized using Photoacoustic Fourier Transform Infrared Spectroscopy (PA-FTIR). A Nicolet Magna IR spectrometer (model 750) equipped with a MTEC (model 300) photoacoustic cell was used. The spectra were collected in the mid-infrared region with 256 scans at a resolution of 4 cm^{-1} and a mirror velocity of 0.158 cms^{-1}. Carbon black was used as a reference and the system was purged with helium gas at a flow rate of 15 cm^3s^{-1}.

Scheme 1. Synthesis of Hybrid-2

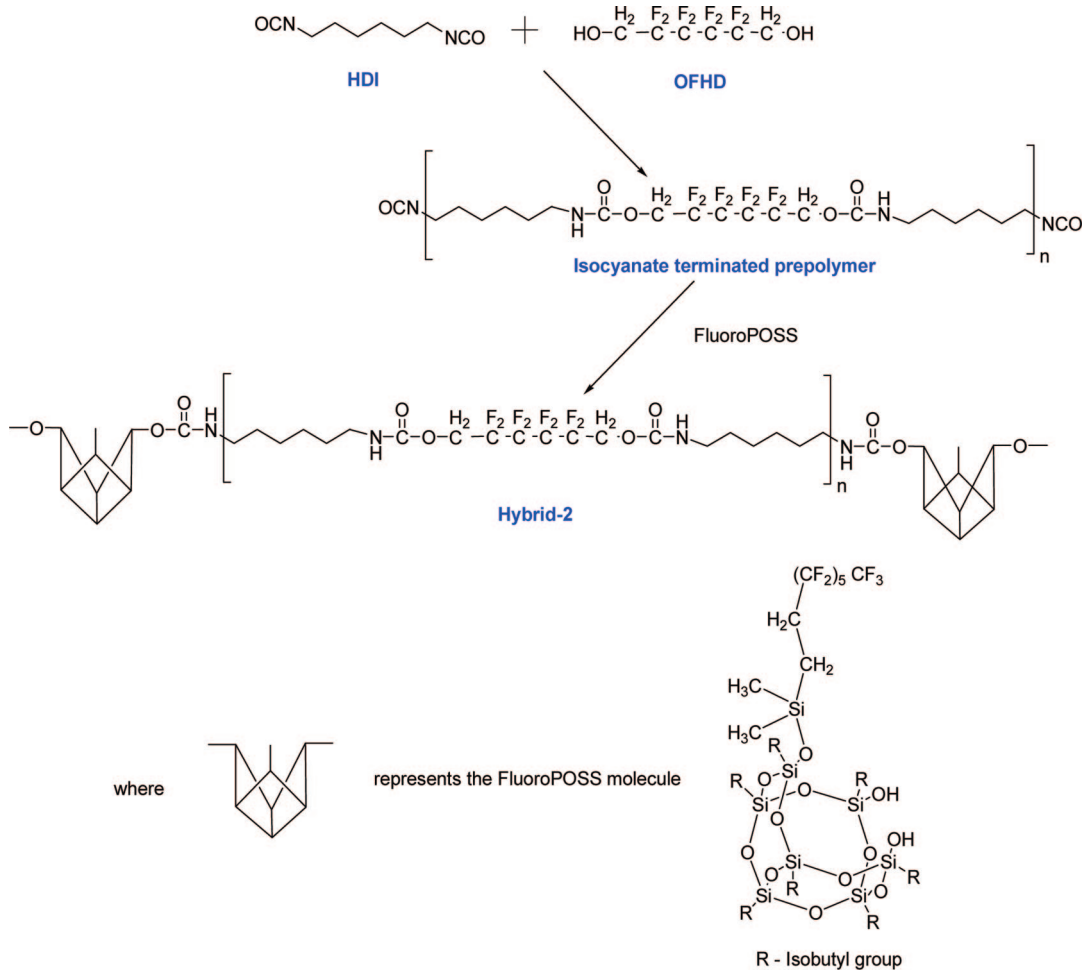

^{29}Si nuclear magnetic resonance (NMR) spectra were recorded on a Varian 300 MHz spectrometer operating at 79.49 MHz and the samples were spun at a frequency of 5 kHz. Chromium(III)acetylacetonate was used as a spin relaxation agent to improve the sensitivity.

Matrix-assisted laser desorption ionization time-of-flight mass spectrometry (MALDI-TOF MS) of the prepolymers and the hybrids were recorded in linear mode using a Micromass M@LDI LR Instrument from Waters (UK) equipped with a pulsed (4 ns) nitrogen laser emitting at 337 nm. The detector was operated in positive ion mode, and the pulse voltage was set to 15 kV. To obtain best spectral resolution, the laser intensity was set at medium to high levels. The matrix was 2,5-dihydroxybenzoic acid (DHB) with acetone as the solvent. Approximately 1 μL of DHB (saturated solution in acetone), 1 μL of sample solution (1 mg mL^{-1}) in hexafluoroisopropanol, and 1 μL of ammonium bicarbonate solution (100 μg mL^{-1}) were mixed and the mixture was dropped onto a stainless steel MALDI-TOF MS plate, and the solvent was evaporated.

Thermal Analysis. Differential Scanning Calorimetry (DSC) of the monomers and the hybrids was performed using a TA Instruments DSC (model 2920) with a heating and cooling rate of 10 °C min^{-1} under nitrogen flow rate of 50 mL min^{-1}. The mass of the sample taken was between 8 to 10 mg and the sample was cycled twice through a temperature range of −100 to 150 °C. Liquid nitrogen was used to achieve subambient temperature.

X-ray diffraction (XRD) analyses of the samples were carried out on a Philips powder X-ray diffractometer using Cu K_α radiation. The 2θ angle ranged from 5 to 40° and the step size and the scan rates were 0.02 and 5° min^{-1}.

Surface Characterization. Atomic force microscopy (AFM) was used to characterize the topography and phase of the thin films coated on silicon wafer. A Multimode AFM with Nanoscope III controller (Veeco Instruments Inc.) was used in tapping mode using silicon tips with curvature radius of 10 nm and spring constant of 10 N/m^{-1}. AFM studies were conducted in air at room temperature. The surface roughness values were evaluated using nanoscope version 5.30 r3 image analysis software.

Advancing and receding contact angles were determined using a Dataphysics OCA 20 contact angle meter employing distilled, deionized water as the reference liquid. Five independent measurements were carried out and the average contact angle is reported.

X-ray photoelectron spectroscopy (XPS) was carried out using Kratos Axis Ultra Spectrometer, equipped with an Al K_α X-ray source ($h\nu$ = 1486.7 eV). The hybrid thin films were characterized at a photoelectron takeoff angle of 90° to the sample surface. Charge correction was performed by fixing the hydrocarbon component of C 1s peak to 284.5 eV. Atomic weight percents for carbon, fluorine, nitrogen, oxygen, and silicon were also calculated from XPS. Elemental analyses (C, N, and F) were performed on the bulk hybrid-1 and hybrid-2 samples through Campbell Microanalytical Laboratory, University of Otago, New Zealand. The error limit in the element composition analyses is ±0.1 %.

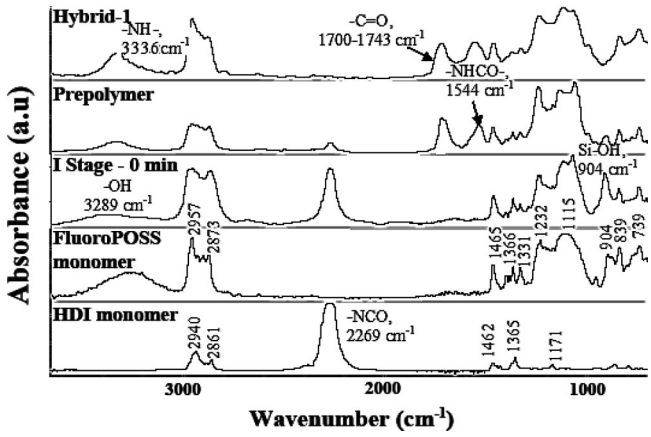

FIGURE 1. FTIR spectra obtained during the synthesis of hybrid-1 at different reaction times.

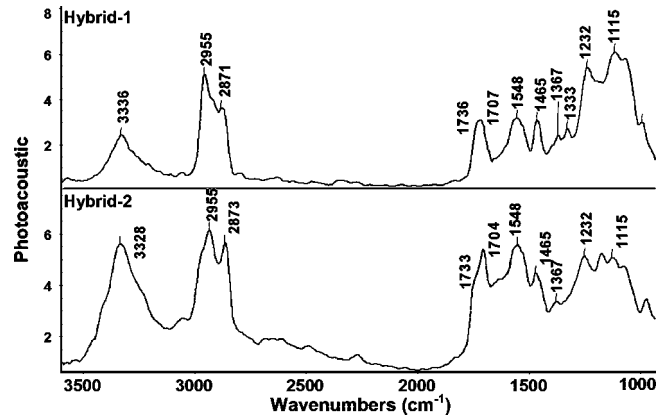

FIGURE 2. PA-FTIR spectra of the hybrids.

RESULTS AND DISCUSSION

Spectroscopic Characterization. The synthesis of hybrid-1 was monitored via transmission FTIR and the spectra of the HDI monomer, fluoroPOSS monomer, initial solution mixture, the prepolymer solution and the final hybrid solution are shown in Figure 1. HDI monomer shows an intense peak at 2269 cm^{-1} (-NCO peak) and other peaks at 2940 cm^{-1} (asymmetric stretching of CH_2), 2861 cm^{-1} (symmetric stretching of CH_2), 1462 cm^{-1} (CH_2 scissors), 1365 cm^{-1} (CN stretch), and 1171 cm^{-1} (CH_2 twist). FluoroPOSS monomer shows a distinct peak at around 1115 cm^{-1}, which arises from Si−O−Si network in the cage structure and a broad peak (3100 cm^{-1} − 3550 cm^{-1}) indicating the presence of Si-OH groups. The peak at 1331 cm^{-1} is attributed to C−F stretching of CF_3 group and the bands at 1232 cm^{-1} and 1169 cm^{-1} are assigned to symmetric and asymmetric stretching of CF_2 groups respectively. Also, the peaks at 904, 839, and 739 cm^{-1} are attributed to Si-OH, Si-CH_2 rocking, and CH_2 deformation, respectively. The peaks corresponding to HDI and fluoroPOSS are present in the initial solution mixture. During the synthesis of the isocyanate terminated prepolymer, the strong peak at 2269 cm^{-1} corresponding to the isocyanate group decreases progressively with time. Also, the broad band in the region of 3100−3550 cm^{-1} due to -OH deformation decreases and a new peak appears at 3336 cm^{-1}, which corresponds to the stretching band of the urethane amide (15, 20). Apart from the peak at 3336 cm^{-1}, two new peaks at 1544 cm^{-1} and a broad peak at 1700−1743 cm^{-1} appear during the course of the reaction. These peaks are assigned to bending of the amide and carbonyl group stretching of the urethane linkage (20) respectively. The urethane carbonyl peak was deconvoluted into two peaks centered at 1736 cm^{-1} and 1707 cm^{-1}, which are assigned to free and hydrogen-bonded urethane carbonyl groups, respectively (21, 22), because of the reaction of the isocyanate group of HDI with the hydroxyl group of fluoroPOSS. The completion of the prepolymer reaction was determined from the disappearance of the hydroxyl peak of FluoroPOSS in the region of 3100−3550 cm^{-1}. The chain extension of isocyanate terminated prepolymer was carried out by further reacting it with OFHD. As the second stage reaction proceeds, the peaks at 2269 and 3500 cm^{-1} due to isocyanate and hydroxyl groups, respectively, decrease and disappear completely. Thus, the FTIR spectra show the consumption of the isocyanate group by −OH groups in fluoroPOSS and OFHD successively to form polyurethane network and the subsequent incorporation of fluorocarbon chain and fluoroPOSS in the polymer main chain structure. The consumption of isocyanate with reaction time was calculated from the decrease in peak height of 2269 cm^{-1} (Figure 1) and is given in the Supporting Information, which shows initial rapid consumption of isocyanate followed by a slow consumption, especially after 70% consumption.

Figure 2 shows the PA-FTIR spectra of hybrids 1 and 2. As discussed earlier, the isocyanate and hydroxyl peaks are completely absent in both hybrids, whereas new peaks are formed corresponding to amide, non-hydrogen bonded and hydrogen-bonded urethane carbonyl and urethane amide bands respectively. The bands corresponding to −Si−O−Si− and fluorocarbon chain remain unchanged in the final hybrids. The only difference between the two prepared hybrids is the intensity and position of the peak corresponding to urethane carbonyl and amide groups. Hybrid-1 shows a broad peak (1700−1743 cm^{-1}), whereas the hybrid-2 sample displays a sharp peak at 1704 cm^{-1} with a shoulder peak at 1733 cm^{-1}. The intensity of the non-hydrogen bonded urethane carbonyl is much lower in hybrid-2 than in hybrid-1. For hydrogen bonding to occur in the hybrid, the molecular segments should come close enough to induce intermolecular interaction. The presence of the fluoroPOSS compounds in the main chain of hybrid-1 will have a different degree of intermolecular interaction and control of the chain motion than that of hybrid-2, where fluoroPOSS is used as chain extender. This reduces the ability to form hydrogen bonding in hybrid-1. Hence, hybrid-2 has higher fractions of hydrogen-bonded urethane carbonyl than hybrid-1. The magnitude of the frequency shift of the free to hydrogen bonded carbonyl is a measure of the hydrogen bond strength (23). It is interesting to note that the shifts of the free to hydrogen-bonded carbonyl frequency are the same (29 cm^{-1}) for both hybrids. The constancy of the frequency shifts, therefore, indicates that the position of fluoroPOSS in the hybrid structure has little effect on the hydrogen-bonding strength between urethane NH and C═O

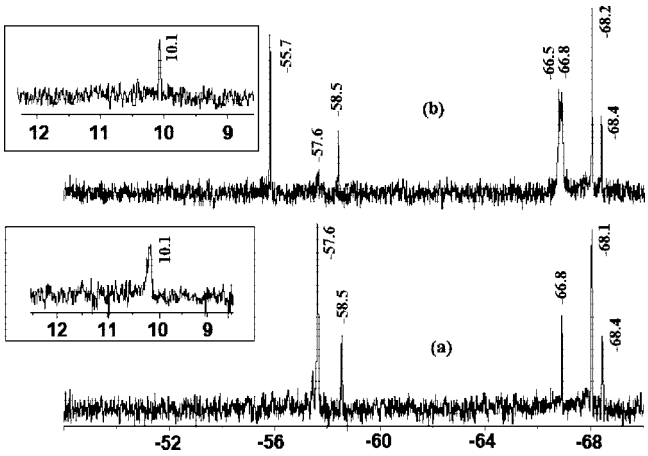

FIGURE 3. ^{29}Si NMR spectra of (a) FluoroPOSS monomer and (b) hybrid-1 prepolymer samples and the inset boxes show the spectra in the region of 9−12 ppm.

groups. This shows that the nature of intermolecular interaction is similar and the extent of the interaction is different for these hybrids. The prepared hybrid samples are not soluble in the original solvent (THF) and most other organic solvents such as toluene, chloroform, dimethylformamide, and dimethylacetamide, indicating the solvent resistance characteristic of the network structure. However, they are soluble in special fluorocarbon-chain-containing solvent such as hexafluoroisopropanol.

^{29}Si NMR spectroscopy was carried out to elucidate the reaction of fluoroPOSS with diisocyanate. Panels a and b in Figure 3 show the expanded ^{29}Si NMR spectra of the fluoroPOSS monomer and the prepolymer of hybrid-1 sample in the region of −48 to −70 ppm and the inset boxes show the spectrum in the region of 8 to 12 ppm respectively. FluoroPOSS monomer shows peaks at three different characteristic regions of −66 to −69, −57 to −59, and 9 to 11 ppm. These regions, in general correspond to T^3 [$(RSi(OSi)_3]$, T^2 [$(RSi(OH)(OSi)_2]$, and M-type [R_3SiOSi] silicon atoms, respectively (15, 20, 24, 25), where R is an organic group. The T^3 region consists of three peaks at −66.8, −68.1 and −68.4 ppm respectively. The four T^3 Si atoms in fluoroPOSS result in more than one resonance band due to different proximity of the Si atoms to the T^2 hydroxyl groups (26). The different proximity of silicon atoms within the cage structure to the opening creates differing amounts of ring strain. This difference in the ring strain causes the chemical shift between T^3 Si atoms. The silicon atom responsible for the more positive resonance band at −66.8 ppm is the one that undergoes most deshielding, which is the Si farthest away from the opening in the cage structure. The T^2 region in fluoroPOSS monomer shows two peaks at −58.5 and −57.6 ppm. Generally, the Si-OH groups in the POSS molecules show resonance peak in the region of −57 to −61 ppm (27, 28). The peak at −57.6 ppm is assigned to the silicon atoms functionalized with hydroxyl groups, which are connected to two siloxane bonds each. The other peak in the T^2 region (−58.5 ppm) of fluoroPOSS monomer possibly originates from more strained T^3 silicon atom, which is connected to the fluorocarbon chain through M-type silicon atom. The presence of a long fluorocarbon chain would produce a highly strained Si−O−Si linkage. This increase in ring strain would cause a positive chemical shift and thus can be responsible for the T^3 resonance band in the usual T^2 resonance region (−58.5 ppm) (26). The ^{29}Si NMR spectrum of fluoroPOSS monomer also shows a peak at 10.1 ppm, which is characteristic to M type silicon atom. This peak arises from the $Si-O-(Si-(CH_3)_2)-$ group linking fluorocarbon chain to the cage structure.

The spectrum of the hybrid-1 prepolymer sample shows the appearance of two new resonance bands at −55.7 and −66.5 ppm (compared to the FluoroPOSS monomer) and the intensity of the T^2 resonance peak at 57.6 ppm corresponding to silicon atoms containing hydroxyl groups is significantly decreased. The other resonance bands from the FluoroPOSS monomer are present in the hybrid prepolymer, indicating that the FluoroPOSS open-cage structure remains intact during the course of the reaction. The peak at 10.1 ppm corresponding to M-type silicon atom is also present in the prepolymer spectrum (shown in inset box), indicating that the fluorocarbon chain attached to the cage structure remains intact. The decrease in the intensity of the peak at −57.6 ppm indicates the utilization of functional hydroxyl groups during urethane formation. A very small proportion of functional hydroxyl groups remain unreacted. As a result, the urethane linkage connected to a silicon atom produces new T^2 type silicon. Therefore, we assign the new resonance band at −55.7 ppm to T^2 silicon arising from deshielding due to the urethane linkage (15). The new peak at −66.5 ppm is assigned as T^3 silicon band (less-strained than the band at −58.5 ppm), resulting from urethane reaction. These results confirm the formation of urethane linkage between FluoroPOSS and diisocyanate.

MALDI-TOF MS was done to measure the molecular weight of the synthesized polymers. On the basis of the composition of the reactant monomer, which primarily contains fluoroPOSS (P), HDI (I), and OFHD (D), the major repeat unit of hybrids 1 and 2 would be $(IP)_n$ and $(ID)_n$, respectively. Panels a and b in Figure 4 show the MALDI-TOF MS spectra of hybrid-1 and hybrid-2 samples along with their prepolymer sample spectra in the inset boxes. The main oligomeric species found in hybrid-1 and hybrid-2 spectra are given in Table 1 along with their theoretical and experimental masses (*m*/*z*). The peaks present below 500 *m*/*z* have resulted from the matrix material, as evidenced from the matrix background spectrum. Hence, these peaks are not taken into consideration. The positive MALDI-TOF MS spectrum of Hybrid-1 shows major peaks at *m*/*z* 1627, 2056, 2989, and 3423, which can be grouped into two distributions with a repeating unit of 1363 *m*/*z* corresponding to the molar mass of $(IP)_n$ repeat unit. It can be observed that the oligomer $(IP)_nD$ bearing prepolymer repeating unit with short fluorocarbon chain derived from fluorodiol as end group is the predominant species (*m*/*z* at 1627 and 2989 with *n* values of 1 and 2, respectively). Another series of peaks (*m*/*z* 2056 and 3423) representing oligomer $ID(IP)_nD$ containing linear fluorourethane chain at either ends of

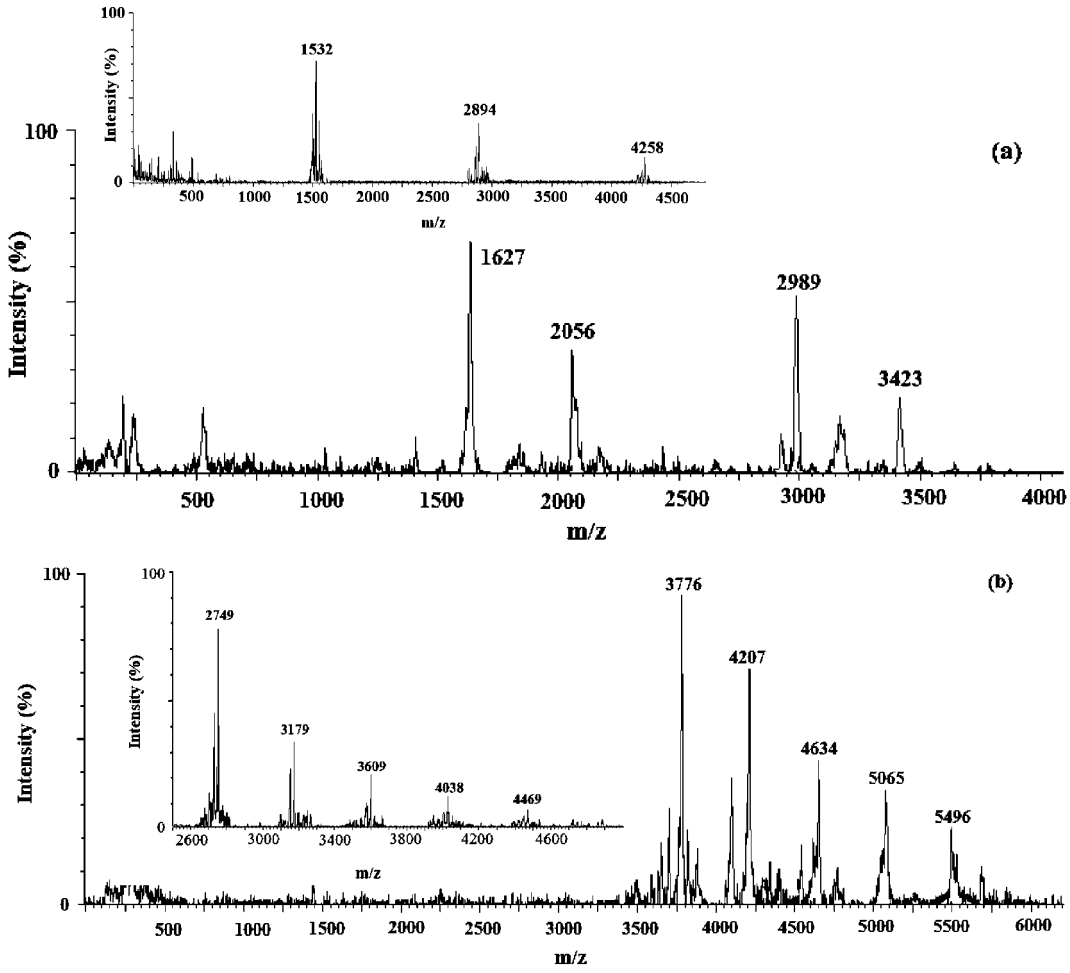

FIGURE 4. MALDI-TOF MS spectra of (a) hybrid-1 and (b) hybrid-2 samples and the inset boxes show their corresponding prepolymer sample spectrum.

prepolymer repeating unit is also present in the spectrum. For further confirmation that the isocyanate terminated prepolymer is formed during the first stage of the reaction, MALDI-TOF MS characterization was performed on the hybrid-1 prepolymer sample. The prepolymer spectrum shows series of peaks with a repeating unit of 1363 *m*/*z* and the end groups determined from the *m*/*z* values of protonated complex confirms the formation of isocyanate terminated prepolymer. Similarly, the prepolymer spectrum of hybrid-2 shows a series of peaks with a repeating unit of 430 *m*/*z* corresponding to isocyanate terminated prepolymer structure of $(ID)_nI$. Hybrid-2 sample shows a series of peaks with a repeating unit of ~430 (*m*/*z*), which corresponds to the mass of the repeating unit in the prepolymer. Based on this, the oligomeric structure corresponding to the major peak can be best illustrated by the oligomeric structure bearing fluoroPOSS as end group. For example, the peak at 4634 (*m*/*z*) can be assigned as the $(ID)_nP$ structure with *n* value of 8. We can also conclude from these spectra that the isobutyl groups and fluorocarbon chain attached to the FluoroPOSS cage structure did not undergo fragmentation. It is also observed from the spectra that there is no evidence of presence of FluoroPOSS as a physical mixture or condensation among themselves. This observation confirms the covalent interaction of hydroxyl groups of FluoroPOSS with diisocyanate from HDI through urethane linkage formation. Among the two hybrids, hybrid-2 forms a relatively higher molecular weight because of the ease with which linear short-chain diol reacts with diisocyanate than with the bulky fluoroPOSS structures.

Thermal Transitions. The DSC thermograms of OFHD monomer, fluoroPOSS monomer, and the final hybrid materials are shown in Figure 5a–c, respectively. The OFHD monomer shows melting peak at around 63 °C and the corresponding crystallization peak during cooling, whereas the fluoroPOSS monomer shows main melting peak at 78.4 °C with a shoulder at 71.3 °C. Interestingly, the crystallization peak was not observed during the cooling stage of this monomer, whereas a glass transition and an exothermic peak are observed during the heating cycle at around −45.4 and 31 °C, respectively. This indicates that during the cooling stage at sufficiently low temperature, some crystal nuclei are introduced, which are trapped in amorphous phase. Hence, this restricts the crystal growth during cooling(29). However, the formed nuclei grow into crystals at the lowest possible temperature (exothermic peak at 31 °C) at a fast rate just after glass-transition temperature due to the increased mobility of the chain segments. Such crystallization by heating from the glassy state is known as cold-

Table 1. Structure of the Predominant Ions and Their Molecular Masses in Hybrid-1 and Hybrid-2 Samples

Sample	Oligomer	Structure	m/z		
			Experimental	Theoretical	n
			Mass of repeating unit = 1363		
			$[M+H]^+$	$[M+H]^+$	
Hybrid-1 Prepolymer	$(IP)_nI$	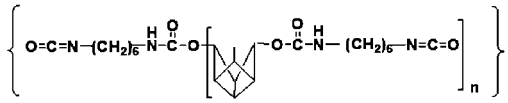	1532 2894 4258	1532 2895 4258	1 2 3
Hybrid-1	$(IP)_nD$	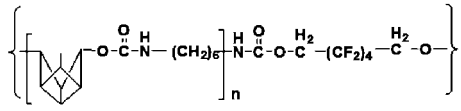	1627 2989	1626 2989	1 2
Hybrid-1	$ID(IP)_nD$	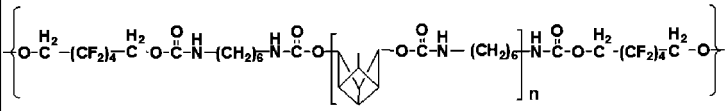	2056 3423	2056 3424	1 2
			Mass of repeating unit = 430		
Hybrid-2 Prepolymer	$(ID)_nI$	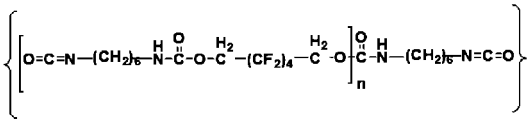	2749 3179 3609 4038 4469	2749 3179 3609 4039 4469	6 7 8 9 10
Hybrid-2	$(ID)_nP$	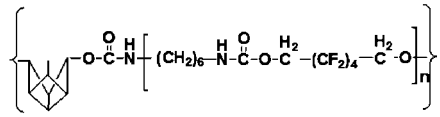	3776 4207 4634 5065 5496	3776 4206 4636 5066 5496	6 7 8 9 10

crystallization, which is observed in very few materials such as polyethyleneterepthalate, polytetrafluoroethylene, and polydiethylsiloxane(29).

In the case of hybrids, no melting or crystallization peak is observed. Instead, hybrid-1 and hybrid-2 show glass transition (T_g) at 18 and 25 °C, respectively. Hence, the most attractive feature of the hybrid materials is their amorphous nature, although both the precursors are crystalline. This result shows that the crystallinity of the OFHD monomer and FluoroPOSS monomer is suppressed by its covalent attachment to the organic polymer chain and thereby suppressing the crystal growth(30, 31). The resultant hybrids show no distinct phase separation as normally observed in PU with hard and soft segments. This can be attributed to the presence of fluorinated segment on both the components, which increases the compatibility between these two precursors(32). Among the two hybrids, hybrid-2 exhibits slightly higher T_g than hybrid-1 sample. The increase in T_g in hybrid-2 can be attributed to the presence of hydrogen bonding between interchain urethane carbonyl and van der Waals interaction of the adjacent fluorocarbon chains as observed from FTIR results.

To confirm the DSC results indicating the amorphous nature of the hybrids, X-ray diffraction (XRD) study was carried out on fluoroPOSS monomer and the hybrid samples and their corresponding XRD patterns are given in Figure 6. The fluoroPOSS monomer shows sharp diffraction peaks indicating a long-range 3D crystalline structure and the main peaks are summarized in Table 2. The spectrum shows four main reflections at 6.28, 10.12, 12.48, and 21.58, which correspond to lattice spacings of 14.12, 8.77, 7.12, and 4.14 Å, respectively. Earlier studies using single-crystal X-ray diffraction, indicates that, in all of the alkyl silsesquioxane structures, the spherical shaped POSS molecules pack in hexagonal structures (33, 34). Moreover, the current result shows that the structures in this family of molecules have features, which are also shared by the new fluoroPOSS materials. However, when fluoroPOSS is hybridized to form urethane linkage, the diffraction patterns are featureless, showing only broad amorphous nature in the low angle. This broad nature of the diffraction pattern indicates that the fluoroPOSS components are evenly dispersed and reacted without any aggregation (35). This observation reveals the absence of any long-range ordering or crystal growth in the formed hybrid, which confirms that the introduction of urethane linkage significantly modifies its crystalline fraction. The hybrid sample shows a small sharp peak at 14.14°, which corresponds to the lattice spacing of 6.28 Å. Because a similar peak is observed in fluoroPOSS monomer sample, this peak is attributed to the distorted anisotropic ordering of fluoroPOSS in the hybrid. This shows that the crystal

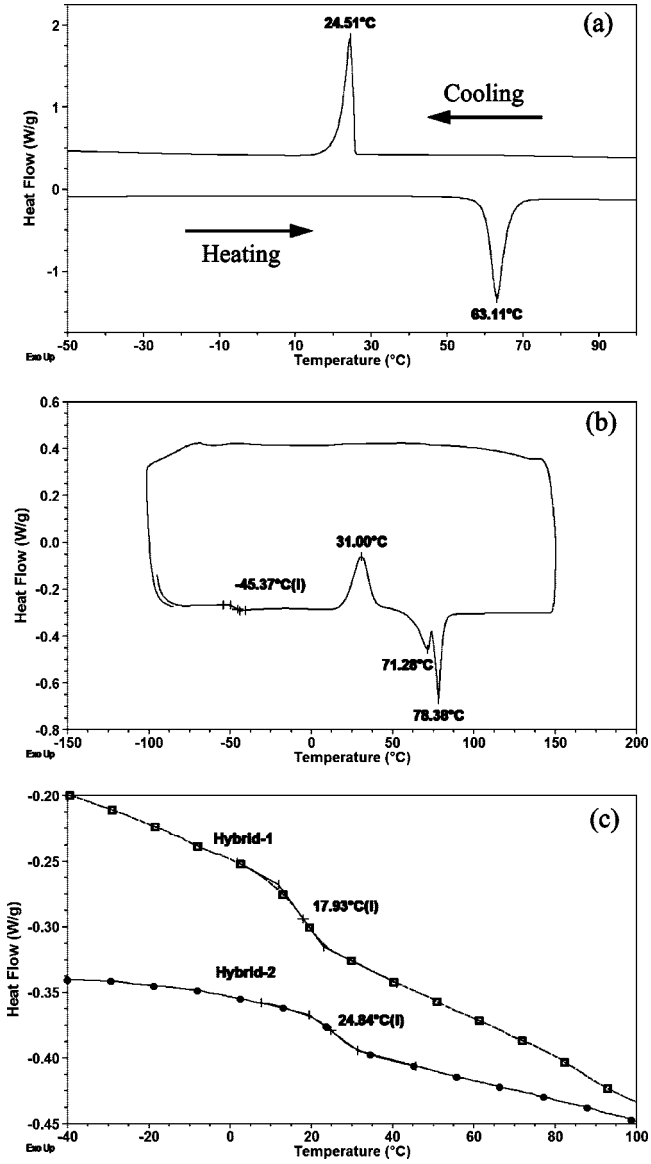

FIGURE 5. DSC thermogram of (a) OFHD monomer, (b) fluoroPOSS monomer, and (c) hybrids.

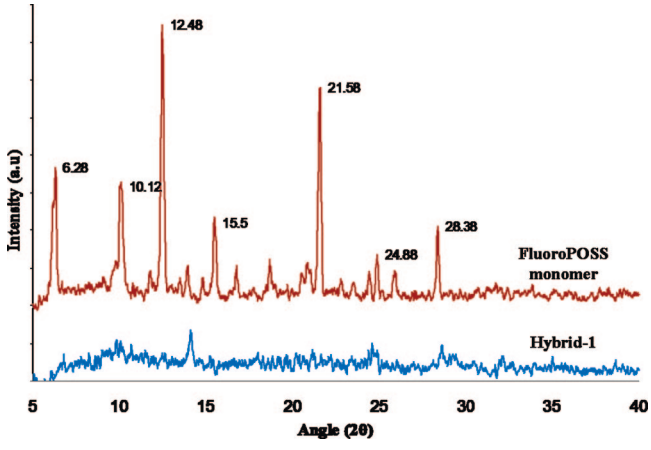

FIGURE 6. XRD spectra of fluoroPOSS monomer and hybrid-1.

development in three dimensions is impossible because of the spatial constraints due to polymer attachment, which results in one-dimensional nanocrystal(34).

Table 2. XRD main reflection angles of FluoroPOSS monomer and their corresponding lattice spacings

angle (2θ)	d spacing (Å)
6.28	14.12
10.12	8.77
12.48	7.12
14.4	6.28
15.5	5.74
21.58	4.14
24.88	3.59
28.38	3.15

Morphological Characterization. Surface morphologies of the hybrid films and FluoroPOSS films were examined by AFM. Figure 7 shows the 3-dimensional topographic images of cleaned silicon wafer, FluoroPOSS, hybrid-1 and hybrid-2 thin films coated on silicon wafer. The surfaces of silicon wafer and fluoroPOSS thin film are relatively smooth with the root-mean-square (rms) roughness values of 0.44 and 1.07 nm, respectively. In contrast, hybrid-1 and hybrid-2 show rougher surface with rms roughness of 6.15 and 5.40 nm (bright area), respectively. Hybrid-1 film shows slightly higher surface roughness in comparison to hybrid-2 thin film surface. This shows increased phase mixing of fluorinated diol with fluoroPOSS in the hybrid-2 sample than in the hybrid-1 sample. Also, surface roughness can be used as an approximate measure of surface free energy (36). For instance, lower surface free energy would expose higher surface area by forming nanoscale features such as nanoscale phase separated fluorinated domains. Both the hybrid surfaces show much higher roughness than FluoroPOSS and silicon wafer surfaces, indicating low energy surface. The formation of fluorine-rich domain morphology is evident from the images of both hybrids, which has resulted from the formation of the 3D network; without that, a featureless surface would result. The large difference in the wettability (hence surface energy) of the fluorinated segment from the nonfluorinated part is the driving force for the surface segregation of the fluoro-segments.

Here, both fluorodiol and FluoroPOSS contain fluorinated chains, which make their surface mobility more competitive and complex (37). Although the majority of bulk analyses of the two hybrids show marginal differences in behavior, the surfaces of the hybrid films exhibit different structures indicating the organization of fluorodomains on the air–hybrid film interface in a different fashion. Also, phase images of hybrid-1 and hybrid-2 (images a and b in Figure 8) corresponding to the topographic images c and d in Figure 7, respectively, are different in nature. For hybrid-1, more discrete domain is uniformly dispersed on the surface, while for hybrid-2 with terminal fluoroPOSS group, a uniform network structure is clearly evident. This shows the different nature of aggregation of fluorosegments on the surface resulting in fluorine-rich domains. The domain sizes were calculated from the line scans of the phase images. The hybrid-1 shows brighter domains of size 70–120 nm, whereas the bright domains in hybrid-2 are in the range of 40–70 nm.

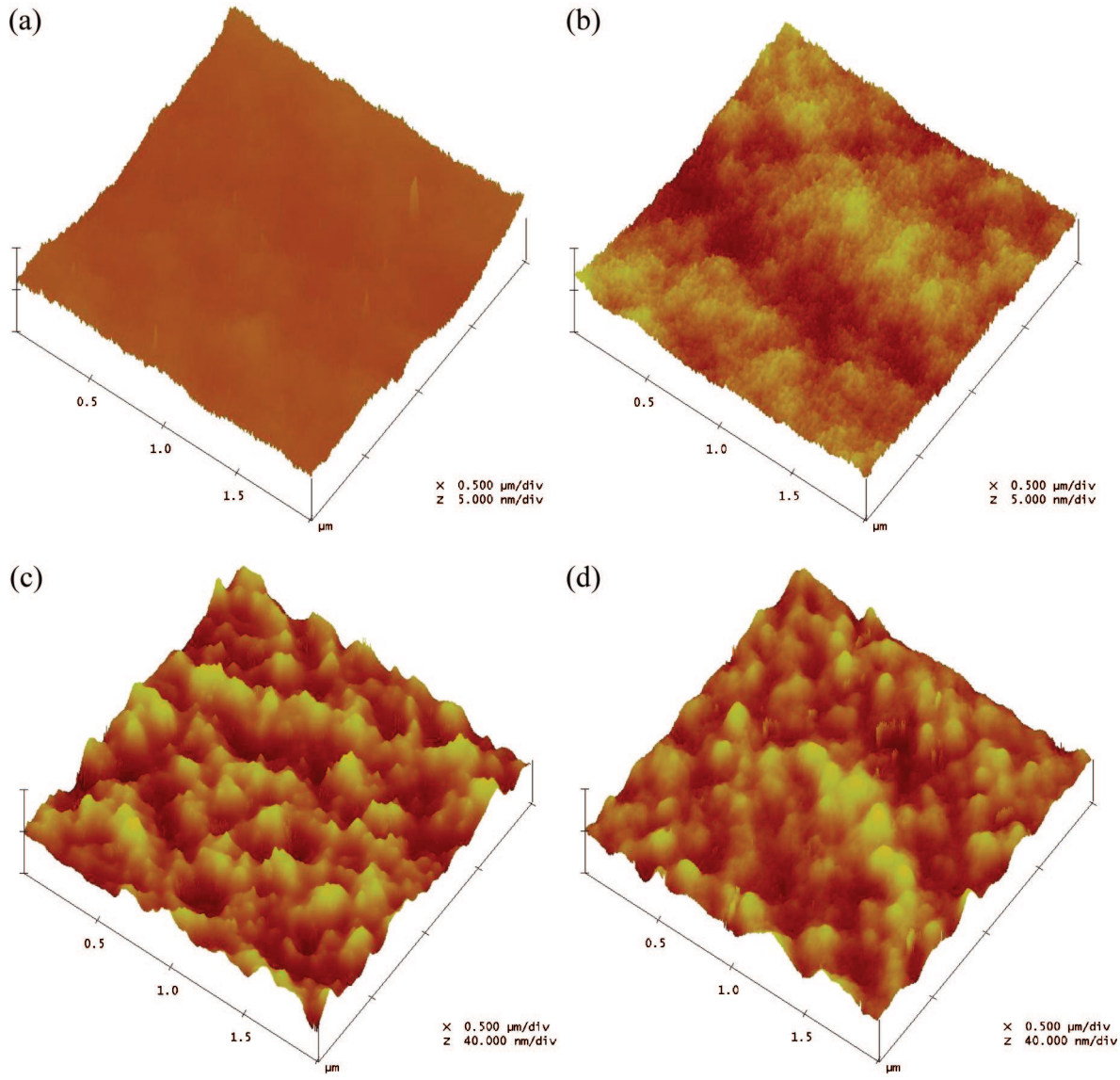

FIGURE 7. 3D topographic images of (a) Si wafer, (b) fluoroPOSS, (c) hybrid-1, and (d) hybrid-2 thin films.

Surface Characterization. To further elucidate surface chemical composition, we carried out structural evaluation of the hybrid films on silicon wafer using XPS. The survey spectrum of hybrid-2 (Figure 9a) shows the presence of silicon, fluorine, carbon, oxygen, and nitrogen, whereas the hybrid-1 shows the presence of all the above-mentioned elements except nitrogen. However, elemental analysis of the bulk hybrid-1 sample (Table 3) shows the presence of nitrogen, which is comparable to the theoretical calculated value. Also, FTIR and NMR spectroscopic results of the samples confirm the formation of urethane linkage. The possible reason for the nondetection of nitrogen in XPS for this system is the fact that the fluorine-rich segment due to its low surface energy rather than the polyurethane matrix migrates toward the thin film−air interface. Also, the accepted depth sensitivity of XPS is 5 nm or less. Hence, the nondetection of nitrogen in hybrid-1 by XPS is attributed to the migration of fluoroPOSS segment to the air-thin film interface. The comparison of the theoretical chemical composition, calculated based on the stoichiometric feed with the bulk and surface chemical composition as determined from elemental analysis and XPS, respectively, are given in Table 3. The migration of fluoroPOSS component to the surface is also confirmed by the amount of fluorine on the surface, which is much higher than both the theoretically calculated value and the bulk value. Hybrid-2 sample also shows higher fluorine content on the surface and much lower values for nitrogen. In general, the hybrid-1 sample exhibits much higher fluorine and silicon content on the surface than the hybrid-2 sample indicating higher migration of fluoroPOSS in hybrid-1 sample. This results in slightly higher surface roughness as observed from topographical images.

The high-resolution spectra of C 1s of both hybrids are given in Figure 9b and Si 2p, O 1s, and F 1s spectra of hybrid-1 are given in Figures 9c−e, respectively. The C 1s spectrum of hybrid-1 shows three peaks centered at 284.5, 291.8, and 294 eV, respectively. The peak at 284.5 eV corresponds to the carbon bound only to carbon and hydrogen (C−C, C−H), whereas the peaks at 291.8 and 294 eV

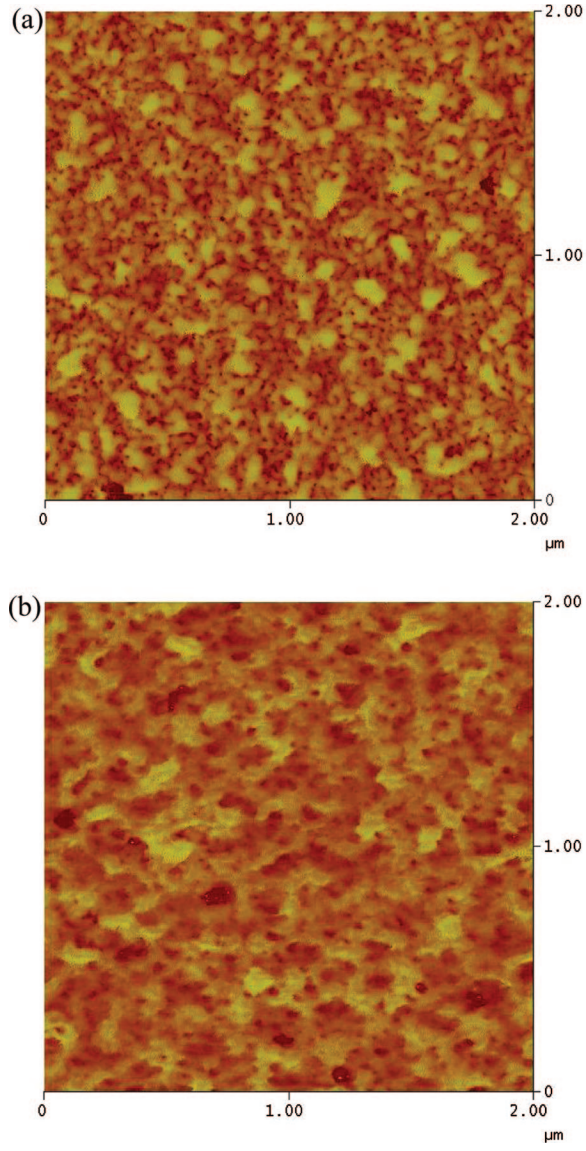

FIGURE 8. Phase images of (a) hybrid-1 and (b) hybrid-2 corresponding to c and d in Figure 7, respectively.

are attributed to CF_2 and CF_3 groups respectively. Usually, the peak corresponding to the carbon making one single bond and one double bond with oxygen (O═C−O) is present at 289.6 eV (38, 39), which is absent in this spectrum. This shows the contribution of carbon from the isobutyl and the long fluoro segments but not from the urethane carbonyl groups. Also, the peak ratio of $C-F_{2/3}$ to C−C/H of hybrid-1 film is 0.13, which is marginally different from the theoretical value of fluoroPOSS (0.18), indicating the predominant presence of fluoroPOSS segments on the surface. This also confirms the migration of fluoroPOSS segments to the surface thereby not detecting the urethane carbonyl and nitrogen peak in hybrid-1 sample. In the case of hybrid-2 film, the high-resolution spectrum of C 1s shows one additional shoulder peak at 285.6 eV and another peak at 289.6 eV. The shoulder peak at 285.6 eV is attributed to the carbon attached to nitrogen, whereas the peak at 289.6 eV is assigned to the urethane carbonyl peak. Another important difference between two hybrid samples is the intensity of the peaks corresponding to fluorocarbon chains and the peak ratio of $C-F_{2/3}$ to C−C/H is 2.44. The major source of C−C/H peak signal is the presence of isobutyl groups on the periphery of fluoroPOSS segments. Much lower intensity of this peak in conjunction with higher fluorocarbon peak indicates the migration of fluorourethane segment on the surface of hybrid-2 film. This is in line with the AFM results, which show the segregation of fluorourethane chains in hybrid-2 film to the surface thereby forming network structure, whereas hybrid-1 film exhibits fluoroPOSS segregation resulting in discrete domain structure distributed on the surface. Although we expect hybrid-2 with terminal FluoroPOSS group to exhibit surface segregation of fluoroPOSS, on the contrary, we observe completely different behavior. Hybrid-1 displays predominant segregation of fluoroPOSS (higher rms ∼ 6.15 nm) and hybrid-2 primarily shows the existence of fluorourethane on the surface. The origin of such surface behavior primarily can result from if hydrophobic association or self-organization occurs through intra or intermolecular aggregation. For hybrid-2, FTIR results show existence of strong intermolecular association (hydrogen bonding between urethane groups of adjacent chains (as shown by FTIR) and van der Waals interaction between fluoro-chains) and the FluoroPOSS groups although in terminal position primarily resides at the substrate−film interface and reveals existence of the fluorourethane segment on the surface. However, hybrid-1 displays just the opposite behavior with predominant self-assembly of fluoroPOSS on the surface and urethane links at the interface. This is ascribed to the prevalent position of the fluoroPOSS segment in the main chain as in hybrid-1, whereas in hybrid-2 with terminal FluoroPOSS, the possibility exists for its bonding at one end to the main chain and for cross-linking with interchain FluoroPOSS or with the substrate in other end due to its terminal nature. The Si 2p peak is centered at 102.6 eV, which corresponds to the $RSiO_n$ in the open cage fluoroPOSS structure. In both hybrids, the O 1s peak is centered at 532.6 eV and is broad in nature, indicating the different states of oxygen. The binding energy of 688.8 eV for fluorine is comparable to the literature values.

The water contact angle measurements were carried out on both the hybrid thin films and the fluoroPOSS thin film coated on silicon wafer using distilled water. Their corresponding contact angles are given in Figure 10. The observed contact angle of the fluoroPOSS thin film is 109°, which is almost same as hybrid-1 (107°) and hybrid-2 (106°), given that PU is quite polar and exhibits contact angle of 65−70° depending on the constituent materials. This shows that the fluoro segments migrates to the surface thereby increasing both the roughness and the hydrophobicity of the hybrid thin film, which also confirms the XPS result. The contact angle is not the only significant parameter determining the hydrophobicity of the film. Also, the surface should show a low level of water drop adhesion (40). Hence, we measured the receding contact angle to understand the adhesion behavior of water drop to the surface. The difference between the measured advancing and receding contact angles of all the

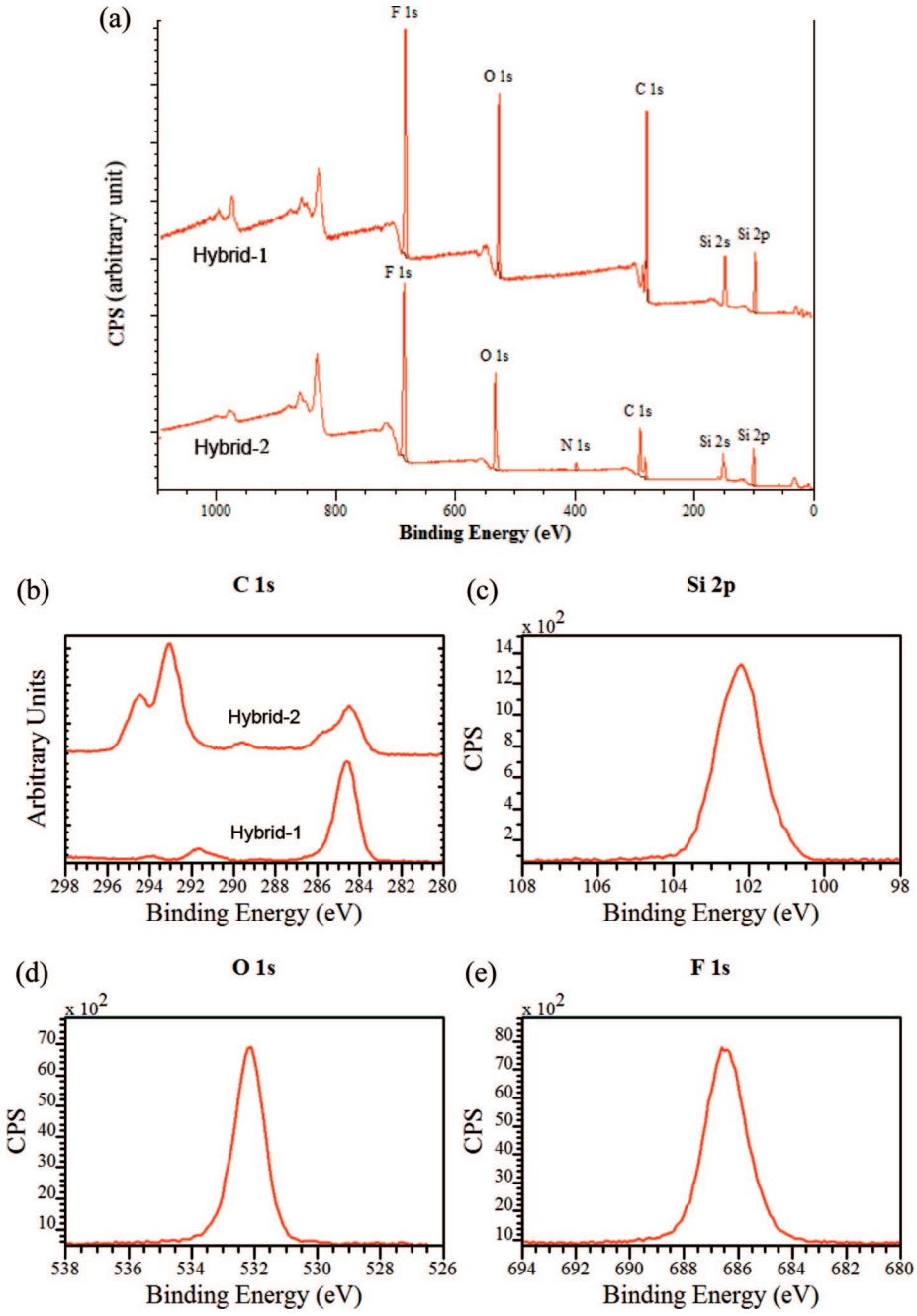

FIGURE 9. (a) Survey spectra and (b) C 1s spectra of hybrid-1 and hybrid-2 thin films, respectively, on silicon wafer; (c–e) Si 2p, O 1s, and F 1s spectra of hybrid-1, respectively.

coated samples are approximately 3 ± 2°. This observation also explains the ultrahydrophobic nature of the surface. An attempt has also been made to determine the oleophobicity of the hybrid films using hexadecane. However, the hybrid films do not exhibit significant oleophobic characteristics. The observed contact angles are 42 ± 3°.

As the thin film formation process on the wafer surface occurs from the prepolymer solution, the evaporation of solvent can induce two conflicting effects: (a) increase in viscosity and (b) migration of fluorinated component with the network formation. The major components used being fluorinated in nature and also of low molecular weight, the system is miscible during curing condition without phase separation. Although the surface roughness is higher for the

Table 3. Comparison of the Surface Chemical Composition Determined by XPS with the Theoretical Value and the Bulk Composition from Elemental Analyses

		% composition			
		hybrid-1		hybrid-2	
element	theoretical (%)	bulk	surface	bulk	surface
C	42.67	44.1	38.16	42.2	46.98
F	23.65	19.7	26.34	20.5	31.39
N	3.31	3.9	0	4.6	1.38
Si	13.27		15.66		8.64
O	17.07		19.84		11.61

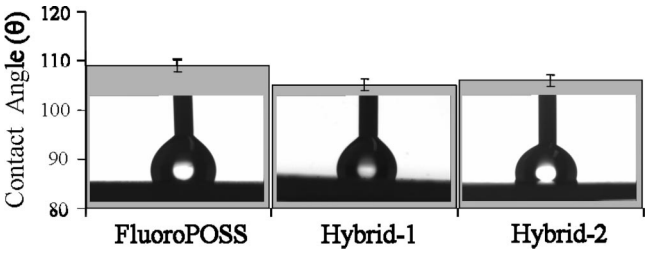

FIGURE 10. Contact angle measurements using distilled water (data at 96.5% confidence level).

hybrid coated samples in comparison with fluoroPOSS-coated samples, it exhibits contact angle more or less in the same range as fluoroPOSS. This observation shows that the surface roughness has a very limited effect on the measured water contact angle. Thus the AFM, contact angle and XPS data reveal the absence of roughness contribution toward hydrophobicity and also confirm that it primarily originates from surface chemical composition of segregated fluoro-segment to the outermost surface.

CONCLUSIONS

We have successfully synthesized a new class of fluoro-POSS-based hybrid polyurethane film with ultrahydrophobic characteristics. FluoroPOSS components retain their partial cage structure in the final hybrids as evidenced from FTIR and NMR spectroscopic analyses. The hybrid films exhibit water contact angle of 107° and low contact angle hysteresis. We have demonstrated that the surface segregation behavior of hydrophobic fluoro component can be controlled by the type and nature of chain extender and resultant hydrophobic association via intra or intermolecular aggregation. The results of AFM, XPS, and contact angle reveal that the ultrahydrophobic behavior achieved is primarily attributed to the formation of low-energy surface formed by the migration of fluoro-segments to the air—-film interface rather than the resulting surface roughness. In one case, the inorganic segment (fluoroPOSS) segregates to the top surface, whereas in the other it resides at the interface. However, both hybrid films show ultrahydrophobicity, which could be driven to superhydrophobicity by further surface roughness variation.

Acknowledgment. The authors gratefully acknowledge the financial support of the Australian Research Council's Special Research Centre for carrying out this work.

Supporting Information Available: Consumption of isocyanate with hybrid-1 synthesis reaction time as determined from FTIR spectra (Figure 1), thermogravimetric analysis data (Figure 2), and DSC curves (Figure 3) showing both heating and cooling cycles (PDF). This material is available free of charge via the Internet at http://pubs.acs.org.

REFERENCES AND NOTES

(1) *Modern Fluoropolymers: High Performance Polymers for Diverse Applications*; Scheirs, J., Ed.; Wiley: Chichester, U.K., 1997; p 660.
(2) Krishnan, S.; Ayothi, R.; Hexemer, A.; Finlay, J. A.; Sohn, K. E.; Perry, R.; Ober, C. K.; Kramer, E. J.; Callow, M. E.; Callow, J. A.; Fischer, D. A. *Langmuir* **2006**, *22*, 5075–5086.
(3) Choudhury, N. R.; Aravindaraj, G. K.; Dutta, N. K. Novel nanocomposites and hybrids for lubricating coating applications. In *Tribology of Polymeric Nanocomposites*; Friedrich, K., Schlarb, A., Eds.; Elsevier: Amsterdam, 2008.
(4) Furstner, R.; Barthlott, W.; Neinhuis, C.; Walzel, P. *Langmuir* **2005**, *21*, 956–961.
(5) Dutta, N. K.; Tran, N. D.; Choudhury, N. R. *J. Polym. Sci., Part B: Polym. Phys.* **2005**, *43*, 1392–1400.
(6) Jeyaprakash, S.; Samuel, J. D.; Ruhe, J. *Langmuir* **2004**, *20*, 10080–10085.
(7) Zhao, N.; Xie, Q.; Kuang, X.; Wang, S.; Li, Y.; Lu, X.; Tan, S.; Shen, J.; Zhang, X.; Zhang, Y.; Xu, J.; Han, C. C. *Adv. Funct. Mater.* **2007**, *17*, 2739–2745.
(8) Ofir, Y.; Samanta, B.; Arumugam, P.; Rotello, V. M. *Adv. Mater.* **2007**, *19*, 4075–4079.
(9) Taylor, R.; Avent, A. G.; Dennis, T. J.; Hare, J. P.; Kroto, H. W.; Walton, D. R. M.; Holloway, J. H.; Hope, E. G.; Langley, G. J. *Nature* **1992**, *355*, 27–28.
(10) Fagan, P. J.; Krusic, P. J.; McEwen, C. N.; Lazar, J.; Parker, D. H.; Herron, N.; Wasserman, E. *Science* **1993**, *262*, 404–407.
(11) Kannan, R. Y.; Salacinski, H. J.; Butler, P. E.; Seifalian, A. M. *Acc. Chem. Res.* **2005**, *38*, 879–884.
(12) Pielichowski, K.; Njuguna, J.; Janowski, B.; Pielichowski, J. *Supramolecular Polymers Polymeric Betains Oligomers*; Advances in Polymer Science Series; Springer: Berlin, 2006; Vol. 201, pp 225—296.
(13) Lichtenhan, J. D. *Comments Inorg. Chem.* **1995**, *17*, 115–130.
(14) Schwab, J. J.; Lichtenhan, J. D. *Appl. Organomet. Chem.* **1998**, *12*, 707–713.
(15) Oaten, M.; Choudhury, N. R. *Macromolecules* **2004**, *38*, 6392–6401.
(16) Tuteja, A.; Choi, W.; Ma, M.; Mabry, J. M.; Mazzella, S. A.; Rutledge, G. C.; McKinley, G. H.; Cohen, R. E. *Science* **2007**, *318*, 1618–1622.
(17) Zeng, K.; Zheng, S. *J. Phys. Chem. B* **2007**, *111*, 13919–13928.
(18) Moody, L. E.; Marchant, D.; Grabow, W. W.; Lee, A. Y.; Mabry, J. M. Determination of Nanocomposite Mechanical and Surface Properties of Semicrystalline Polymer Blends with POSS. In *SAMPE 2005 Fall Technical Conference*; Seattle, Oct 31—Nov 3, 2005 SAMPE: Covina, CA, 2005.
(19) Yoon, S. C.; Ratner, B. D. *Macromolecules* **1988**, *21*, 2401–2404.
(20) Neumann, D.; Fisher, M.; Tran, L.; Matisons, J. G. *J. Am. Chem. Soc.* **2002**, *124*, 13998–13999.
(21) Tai Ho, K. J. W. *Macromolecules* **1992**, *25*, 3521–3527.
(22) Kuo-Yu Chen, J.-F. K. *Macromol. Chem. Phys.* **2000**, *201*, 2676–2686.
(23) Schrems, O.; Oberhoffer, H. M.; Luck, W. A. P. *J. Phys. Chem.* **1984**, *88*, 4335–4342.
(24) Clayden, N. J.; Pernice, P.; Aronne, A. *J. Non-Cryst. Solids* **2005**, *351*, 195–202.
(25) Bein, T.; Carver, R. F.; Farlee, R. D.; Stucky, G. D. *J. Am. Chem. Soc.* **1988**, *110*, 4546–4553.
(26) Matejka, L.; Dukh, O.; Hlavata, D.; Meissner, B.; Brus, J. *Macromolecules* **2001**, *34*, 6904–6914.
(27) Feher, F. J.; Newman, D. A.; Walzer, J. F. *J. Am. Chem. Soc.* **1989**, *111*, 1741–1748.
(28) Feher, F. J.; Soulivong, D.; Nguyen, F. *Chem. Commun.* **1998**, 1279–1280.
(29) Wunderlich, B. The basis of thermal analysis. In *Thermal Characterization of Polymeric Materials*; Turi, E. A., Ed.; Academic Press: New York, 1997; Vol. 1.
(30) Zheng, L.; Hong, S.; Cardoen, G. g.; Burgaz, E.; Gido, S. P.; Coughlin, E. B. *Macromolecules* **2004**, *37*, 8606–8611.
(31) Hillson, S. D.; Smith, E.; Zeldin, M.; Parish, C. A. *J. Phys. Chem. A* **2005**, *109*, 8371–8378.
(32) Tonelli, C.; Ajroldi, G.; Marigo, A.; Marega, C.; Turturro, A. *Polymer* **2001**, *42*, 9705–9711.
(33) Waddon, A. J.; Coughlin, E. B. *Chem. Mater.* **2003**, *15*, 4555–4561.
(34) Zheng, L.; Waddon, A. J.; Farris, R. J.; Coughlin, E. B. *Macromolecules* **2002**, *35*, 2375–2379.
(35) Kim, K.-M.; Adachi, K.; Chujo, Y. *Polymer* **2002**, *43*, 1171–1175.
(36) Jeong, H. Y.; Lee, M. H.; Kim, B. K. *Colloids Surf., A* **2006**, *290*, 178–185.
(37) Tan, H.; Xie, X.; Li, J.; Zhong, Y.; Fu, Q. *Polymer* **2004**, *45*, 1495–1502.
(38) Clark, D. T.; Dilks, A. *J. Polym. Sci., Part A: Polym. Chem.* **1979**, *17*, 957–976.
(39) Laoharojanaphand, P.; Lin, T. J.; Stoffer, J. O. *J. Appl. Polym. Sci.* **1990**, *40*, 369–384.
(40) Chen, W.; Fadeev, A. Y.; Hsieh, M. C.; Oner, D.; Youngblood, J.; McCarthy, T. J. *Langmuir* **1999**, *15*, 3395–3399.

AM800056P